Glass structure and ion dynamics of lead–cadmium fluorgermanate glasses

C. C. Tambelli, J. P. Donoso, C. J. Magon, L. A. Bueno, Y. Messaddeq, S. J. L. Ribeiro, L. F. C. de Oliveira, and I. Kosacki

Citation: The Journal of Chemical Physics **120**, 9638 (2004); doi: 10.1063/1.1712905
View online: http://dx.doi.org/10.1063/1.1712905
View Table of Contents: http://scitation.aip.org/content/aip/journal/jcp/120/20?ver=pdfcov
Published by the AIP Publishing

Glass structure and ion dynamics of lead–cadmium fluorgermanate glasses

C. C. Tambelli, J. P. Donoso,[a] and C. J. Magon
Institute of Physics, USP, P.O. Box 369, 13560-970 São Carlos, SP, Brazil

L. A. Bueno, Y. Messaddeq, and S. J. L. Ribeiro
Laboratory of Photonic Materials–Institute of Chemistry–UNESP, P.O. Box 355, 14801-970 Araraquara, SP, Brazil

L. F. C. de Oliveira
Núcleo de Espectroscopia e Estrutura Molecular, Instituto de Ciências Exatas, UFJF, 36036-330, Juiz de Fora, MG, Brazil

I. Kosacki
Metals and Ceramics Division, Oak Ridge National Laboratory, Oak Ridge, Tennessee 37830

(Received 23 October 2003; accepted 1 March 2004)

Glass structure and fluorine motion dynamics are investigated in lead–cadmium fluorgermanate glasses by means of differential scanning calorimetry, Raman scattering, x-ray absorption (EXAFS), electrical conductivity (EC), and ^{19}F nuclear magnetic resonance (NMR) techniques. Glasses with composition $60PbGeO_3–xPbF_2–yCdF_2$ (in mol %), with $x+y=40$ and $x=10$, 20, 30, 40, are studied. Addition of metal fluorides to the base $PbGeO_3$ glass leads to a decrease of the glass transition temperature (T_g) and to an enhancement of the ionic conductivity properties. Raman and EXAFS data analysis suggest that metagermanate chains form the basic structural feature of these glasses. The NMR study leads to the conclusion that the F–F distances are similar to those found in pure crystalline phases. Experimental results suggest the existence of a heterogeneous glass structure at the molecular scale, which can be described by fluorine rich regions permeating the metagermanate chains. The temperature dependence of the NMR line shapes and relaxation times exhibits the qualitative and quantitative features associated with the high fluorine mobility in these systems. © *2004 American Institute of Physics.* [DOI: 10.1063/1.1712905]

I. INTRODUCTION

It is well known by glassmakers that the addition of fluoride ions to oxide based glass batches leads to pronounced effects on the properties of the resulting glass. Fluorides decrease melting temperatures, contribute to eliminate OH residual groups, decrease refractive index and provide fluorine ion conductivity. From a structural point of view, a typical metal (M) oxide glass network is described by the aperiodic association of basic structural units like the $[MO_4]$ tetrahedral, known to exist in silica or germania based systems. Fluoride anions in these mixed systems can be considered mainly as nonbridging, therefore, the addition of fluoride ions leads to a decrease in connectivity. Part of the fluoride ions in mixed fluoride/oxide glasses, weakly bonded to the glass network, have been identified as the charge carriers in conductivity measurements.[1–6] In fact, the enhanced conductivity observed in different mixed glasses suggested different electrochemical applications such as halide sensors, solid-state batteries and glass purifiers. Besides, these mixed systems have interesting crystallization properties. The so-called ultratransparent glass ceramics, where metal fluorides nanocrystals are identified in the oxide glass host, can be obtained by controlled crystallization treatment.[7–15]

These oxifluoride materials have been studied by different experimental techniques such as optical spectroscopy, transmission electron microscopy, thermal analysis, conductivity measurements, and F(1*s*) x-ray photoelectron spectra.[1–15] Nuclear magnetic resonance (NMR) is a well-known experimental technique to study glass structure and ion dynamics. High resolution and spectral deconvolution NMR techniques have been used to study structural arrangements of metal fluoride glasses.[16,17] Variable temperature NMR line shape and spin-lattice relaxation provide an effective probe for ion dynamics on the microsecond to second time scale.[16–24]

This paper reports the study of cadmium–lead fluorogermanate glasses. These glasses have been proposed before as potential hosts for rare earth containing transparent glass ceramics, but no systematic study of the glass structure was performed.[11] We will see hereafter that the studied glasses display interesting conductivity properties. In fact, enhanced electrical conductivity observed with the addition of lead fluoride (PbF_2) to different oxide glasses seems to be a very general feature, which does not depend on the nature of the oxide glass host.[5]

The general purpose of this report is to build up a picture of the base glass structure. The knowledge of such structural features can offer further support for a better comprehension of the enhanced mobility of fluoride ions observed for similar mixed glasses and, also, to understand the structural

[a]Author to whom correspondence should be addressed. Fax: +55 16 273 9876. Electronic mail: donoso@if.sc.usp.br

TABLE I. Summary of parameters obtained from (a) DSC: T_g is the glass transition temperature, T_x is the onset of the crystallization peak, and T_p is the temperature at the exothermic crystallization peak maximum, (b) EXAFS: N is the number of atoms in the coordination shell at average interatomic distance R from the absorbing atom, as determined from fitting analysis in the region $k=3.88-12.62$ assuming hexagonal monoclinic $PbGeO_3$, and (c) ^{19}F NMR: M_2 is the second moment of the spectra at 173 K and E_A is the activation energy for fluorine motions determined from the $1/T_1$ data in the temperature regions II and III. ρ is the material density.

$PbGeO_3$	PbF_2	CdF_2	ρ (g/cm^3)	T_g (K)	T_x (K)	T_p (K)	N (± 0.5)	R (Å) (± 0.01)	M^2 (G^2) (± 0.5)	E_A (eV)
100	0	0	6.84	643	693	715	4.1	1.74	⋯	⋯
60	40	0	7.66	500	543	569	4.1	1.74	4.1	0.28(II) 0.75(III)
60	30	10	7.40	529	580	604	4.0	1.74	⋯	0.30(II) 0.62(III)
60	20	20	7.17	552	611	636	4.1	1.74	5.7	0.28(II)
60	10	30	6.92	574	715	750	4.0	1.74	⋯	⋯
60	0	40	6.83	594	724	747	4.1	1.74	6.2	0.38(II) 0.63(III)

modifications occurring during heat treatments performed at temperatures above the glass transition temperature (T_g), which leads to transparent glass-ceramics. Measurements include differential scanning calorimetry (DSC), Raman scattering, x-ray absorption (EXAFS), electrical conductivity (EC), and ^{19}F nuclear magnetic resonance (NMR).

II. EXPERIMENT

Glasses with composition $60PbGeO_3-xPbF_2-yCdF_2$ (in mol %), with $x+y=40$ and $x=10$, 20, 30, 40, were prepared by the classical melting ($T=1073$ K for 30 min in open Pt–Au crucibles) and quenching method (to glass transition temperature, T_g, in brass molds) from vitreous $PbGeO_3$, α-PbF_2 (orthorhombic, Aldrich, 99.99%) and CdF_2 (cubic, Aldrich, 99%). Vitreous $PbGeO_3$, was obtained from analytical purity PbO and GeO_2 well mixed and melted in Pt crucibles at 1273 K, followed by quenching to room temperature. The amorphous nature of the glass samples was checked by x-ray diffraction of powdered samples.

Raman measurements were performed for powdered samples using a Micro-Raman set-up from Renishaw, with He–Ne laser excitation (6345 Å).

Impedance measurements were carried out by the ac (two probes) technique, using a Solartron 1260 frequency response analyzer with 1296 interface, which operates in the $0.1-5\times10^6$ Hz frequency range and is capable to measure resistance values up to 10^{10} Ω. All the measurements were performed under air atmosphere in the temperature range of 293–623 K. From the complex impedance data, taken as a function of the electric field frequency, the relative contribution of the bulk, grain boundaries and electrode resistances could be determined. Typical results are represented as a Cole–Cole diagram, composed of three semicircles attributed to the different relaxation times of each response. With the aid of a parallel connected resistor–capacitor equivalent circuit, the diagrams were fitted and analyzed, being the high- and intermediate-frequency semicircles related to the bulk and grain boundary resistances, while the low-frequency semicircle was attributed to the electrode response. The bulk resistance was represented by the high-frequency semicircle and its value, as determined from the fitting of the impedance diagram, was used to calculate the bulk conductivity, hereafter denoted by σ_0.

X-ray absorption (EXAFS) experiments were conducted at the XAFS station of the LNLS (Brazilian National Synchrotron Light Laboratory, www.lnls.br) ring, operating at 1.37 GeV and 100 mA of nominal current with the beam monochromatized by a Si(111) double crystal. Spectra were recorded at the Ge K edge (11104 eV) in the transmission mode with Ar filled ionization chambers in the detection. Powdered samples (grain size <20 μm) were deposited on Milipore membranes (2 μm) with powder quantities adjusted in order to obtain reasonable absorption coefficients.

^{19}F NMR line shapes and spin-lattice relaxation times were measured in the temperature range 100–800 K, using a pulsed NMR spectrometer operating at 36 MHz and equipped with a TECMAG NMR-kit. For measurements, small pieces of the samples were placed inside the 4 mm diam sample tubes and, measurements were performed beginning at the lowest temperature and increasing the temperature up to above T_g. For each run, an individual sample was used. NMR spectra were obtained by Fourier transformation of the averaged free induction decay signal ($\pi/2$ pulse ≈ 2 μs). Spin-lattice relaxation times, T_1, were determined by means of the saturation-recovery pulse sequence. The spin-lattice relaxation time in the rotating frame, $T_{1\rho}$, was measured at 36 MHz for a rotating rf field of about 5 G.

III. RESULTS AND DISCUSSION

Homogeneous and transparent glasses were obtained with no crystallization traces detectable by x-ray diffraction, and exhibiting characteristic temperatures that could be easily identified in the DSC scans (not shown here). Table I summarizes the relevant parameters obtained from DSC analysis. The glass transition temperature, T_g, is observed at 643 K for the vitreous $PbGeO_3$ precursor. With the addition of 40 mol % of PbF_2, T_g decreases to 500 K. The addition of the same amount of CdF_2 to the base glass leads to a less pronounced decrease in T_g (to 594 K). The decrease in T_g salient the modifier activity played by the metal fluorides, consisting of the substitution of nonbridging fluorine atoms

for bridging oxygen atoms. As shown in Table I, T_g is observed in the range 500–594 K for glasses with different amounts of PbF_2 and CdF_2. Earlier studies lead to the conclusion that the network modifier character of PbF_2 in the $SiO_2-PbF_2-CdF_2$ glassy system was much more pronounced, emphasizing the differences in the modifying role played by PbF_2 and CdF_2 in the glass structure.[15]

Concerning the base $PbGeO_3$, an exothermic feature related to devitrification is observed in the DSC scan, peaking at 715 K. Heat treatments performed at this temperature lead to the monoclinic (space group $P2/n$) $PbGeO_3$, isomorphous to the alamosite $PbSiO_3$, whose structure is described by $(GeO_3)_n$ chains with twelve $[GeO_4]$ tetrahedra linked in a repeated unit.[25] With respect to the glass preparation, some additional remarks deserve careful consideration. Starting from GeO_2 and PbO mixtures, submitted to heat treatments at the temperatures for which the phase diagrams state the uniqueness of monoclinic $PbGeO_3$, a mixture of lead germanates with different stoichiometric Pb/Ge ratios were always obtained, even when long lasting heat treatments of about two to three days were employed. Pure monoclinic $PbGeO_3$ could only be obtained by the crystallization, at 715 K, of a glass prepared with that same composition determined from the phase diagram. Such experimental evidence strongly suggests similarities between the $PbGeO_3$ glass and the crystalline monoclinic structures. It also corroborates the model to be proposed hereafter, in which the structure of the lead–cadmium fluorgermanate glasses has many similarities with that of their $PbGeO_3$ precursor.

A. Raman and x-ray absorption

Figure 1 shows the Raman spectra obtained for the crystalline [Fig. 1(a)] and amorphous [Fig. 1(b)] $PbGeO_3$. The main bands, occurring at the same spectral region for both, crystalline and amorphous phases, are inhomogeneously broadened for the glasses. In the high wavenumber region, the bands occurring at 743, 780, and 814 cm^{-1} in Fig. 1(a) could be assigned to the localized Ge–O stretching modes of the polymerized metagermanate structure. The broadband observed for the glass at 794 cm^{-1} [Fig. 1(b)] could also be assigned to the same vibrational modes. The NMR nomenclature used in connection with the germanate compounds classifies the different germanate species as Q^n $(n=0-4)$, where n denotes the number of bridging oxygen atoms for each $[GeO_4]$ basic tetrahedra. With this definition, Q^4 relates to the structure containing only bridging oxygen atoms linked to Ge atoms and, Q^0 to isolated $[GeO_4]$ tetrahedra. In an earlier work we proposed that the bands observed in the Raman spectrum of the vitreous $PbGeO_3$ could be assigned to vibrational modes of Q^2 species,[26] meaning that each $[GeO_4]$ tetrahedron displays two bridging and two nonbridging oxygen atoms. Recalling the spectra of Fig. 1(a), we remark that some lines are observed in the medium wave number range at 442, 487, 508, 559, and 575 cm^{-1}. The broadband centered at 528 cm^{-1}, observed for the glasses in Fig. 1(b), could be interpreted as the envelope of the crystalline phase lines. Stretching vibrational modes of Ge–O–Ge bonds are observed in this region. The bands at low wavenumber could be assigned either to extended vibrational modes or to Pb–O localized modes.

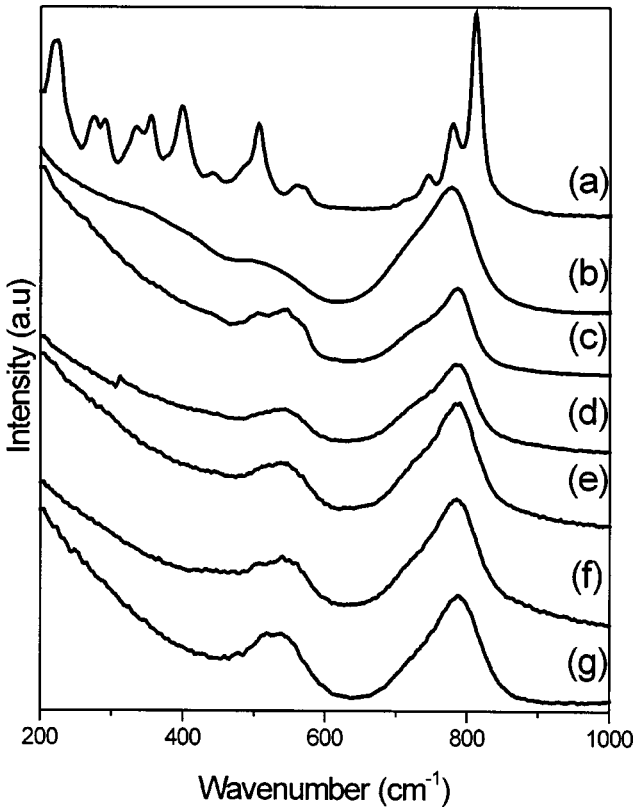

FIG. 1. Raman spectra: (a) PbGeO3–crystal, (b) PbGeO3–glass, (c) 60PbGeO3–40PbF2, (d) 60PbGeO3–30PbF2–10CdF2, (e) 60PbGeO3–20PbF2–20CdF2, (f) 60PbGeO3–10PbF2–30CdF2, and (g) 60PbGeO3–40CdF2.

The only observed change in the spectrum obtained for the $PbGeO_3$ glass, upon addition of lead and cadmium fluorides, is a slight blueshift (≈ 10 cm^{-1}) of the main high wave number band. This increase in band order may be related to depolymerization effects, more easily reflected in the decrease of T_g (Table I). As mentioned before, fluoride addition leads to a decrease in the connectivity of the base oxide matrix with nonbridging fluorine atoms substituting for oxygen atoms. Figures 1(c)–1(g) display the Raman spectra obtained for the five glasses studied here, and all spectra display the broadband peaking at 786 cm^{-1}. Additional results (not shown here) exhibit similar Raman spectra for all samples representatives of the vitreous domain of the system $PbGeO_3-PbF_2-CdF_2$.

X-ray absorption (EXAFS) data obtained at the Ge K edge were analyzed according to the procedure given in Refs. 14 and 15. The general procedure of pre-edge, background removal, normalization and extraction of the $\chi(k)$ EXAFS oscillations was employed. The data were Fourier transformed leading to spectra scaled in distances, and the peaks in the Fourier transforms, corresponding to particular coordination shells, were filtered and back-transformed to k-space. The resulting EXAFS-filtered signal was treated as a sum of sinusoidal wave functions using single scattering approximation.[27] Table I shows the obtained results. Four

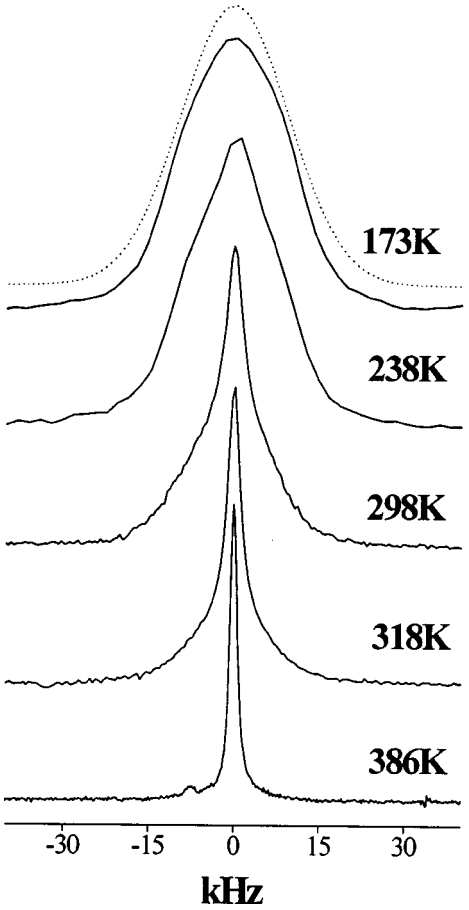

FIG. 2. Typical ^{19}F NMR spectra of the glass $60PbGeO_3-20PbF_2-20CdF_2$ at indicated temperatures. All spectra were measured at the Larmor frequency of 36 MHz. The dashed spectrum corresponds to the Gaussian fitting of the line shape at 173 K.

coordinated oxygen atoms, at a mean distance of 1.74 Å, were determined for Ge atoms in all samples.

The fourfold oxygen coordination of Ge atoms, as determined by EXAFS, leads to the conjecture that metagermanate chains, similar to those found in the $PbGeO_3$ crystallized glass, constitute an important feature of the lead–cadmium fluorgermanate glass structure. This finding is consistent with the Raman results shown in Fig. 1. EXAFS data obtained here could not distinguish between oxygen and fluorine atoms, but some depolymerization effects due to the substitution of terminal fluorine atoms for bridging oxygen atoms is also clear from Raman and DSC measurements.

B. ^{19}F nuclear magnetic resonance

1. Static spectra

The temperature dependence behavior of the ^{19}F NMR spectra of the samples are similar, and Fig. 2 shows typical results obtained with the glass $60PbGeO_3-20PbF_2-20CdF_2$. Fluorine nuclei ($I=\frac{1}{2}$) have a large gyromagnetic ratio, $\gamma_n/2\pi=40.055$ MHz/T, and 100% natural abundance. The absence of ionic motion at low temperatures (a temperature region commonly referred as the rigid network) causes the ^{19}F resonance spectrum to be inhomogeneously broadened due to dipole–dipole couplings between neighboring spins, resulting in an approximated Gaussian line shape. Considering that the nonzero nuclear spins, ^{207}Pb, ^{111}Cd, ^{113}Cd, ^{73}Ge, and ^{17}O have small gyromagnetic ratios or low natural abundance, we can assume that the $^{19}F-^{19}F$ dipole–dipole interaction is the main source of the line broadening at low temperatures. The Van Vleck second moment of the Gaussian line shape, M_2, can be used to estimate the strength of the nuclear dipolar coupling, which is inversely proportional to the sixth power of the internuclear distances.[28] The experimental determination of the second moments has been used to estimate average internuclear distances in glasses.[19,28,29]

The low temperature fluorine second moments estimated from the Gaussian fitting of the NMR spectra (at $T=173$ K) are shown in Table I. It is interesting to draw comparisons between the obtained M_2 values with those reported in the literature for corresponding fluoride crystals. For example, the value $M_2=4.1\ G^2$, obtained for the glass with composition $60PbGeO_3-40PbF_2$ compares well with the one reported for crystalline β-PbF_2, where the F–F distance is 2.97 Å and $M_2=4\ G^2$.[30] A value of $6.2\pm0.5\ G^2$ was obtained for the glass with composition $60PbGeO_3-40CdF_2$ and this value compares with the second moment calculated for CdF_2 ($M_2=6.5\ G^2$) where the F–F distance is 2.7 Å. Finally, the result obtained for $60PbGeO_3-20PbF_2-20CdF_2$ ($M_2=5.7\pm0.6\ G^2$) is consistent with the second moment calculated for solid solutions $Cd_{1-x}Pb_xF_2$, where M_2 is in the range $3.8-6.5\ G^2$. In this last case the lattice constant was found to depend linearly on composition, from $a=5.927$ Å for $x=0$ to $a\approx5.94$ Å for $x=1$.[31]

From these comparisons it is possible to affirm that the fluorine ions are not uniformly distributed through the entire structure of the material. This conclusion can be corroborated by a simpler argument, as follows. Taking into account the density (Table I) and the nominal composition of the $60PbGeO_3-40PbF_2$ glass, the number of fluorine atoms per cm^3 of the glass is $n=1.25\times10^{22}$. If we suppose, just for the sake of argument, that these atoms are homogeneously distributed, corresponding to maximized F–F distances of $(1/n)^{1/3}=4.3$ Å, the resulting fluorine second moment estimated from the Van Vleck method should be $0.42\ G^2$, which is one order of magnitude smaller than the experimental value obtained for this glass ($M_2=4.1\ G^2$). Similar conclusion can be drawn for the other glass compositions. Taking into account the similarity of the fluorine second moment in both materials, $60PbGeO_3-40PbF_2$ glass and crystalline β-PbF_2, the average F–F distance in the glass is estimated to be ≈3 Å.

To explain these results, we can recall the description of the glass structure proposed on the basis of Raman and EXAFS measurements, in which the metagermanate chains are forming the basic element of the microscopic glass structure, with some nonbridging fluorine atoms substituting oxygen atoms. NMR results provide additional evidence that fluorine rich regions are permeating metagermanate chain structures, in which, F–F distances are comparable to those found in crystals. These arguments imply that fluorine phases are distributed in microdomains at the interface of the amorphous network formed by the metagermanate chains, with a

local order similar to that of the corresponding crystal. This assumption can explain most of the present experimental data and can well account for the interesting and particular crystallization properties of these oxyfluoride glasses,[7,15] in which the nucleation of a fluoride crystal would be energetically favored in those fluorine-rich regions.

2. Motional line narrowing

The ionic conduction in these glassy materials is promoted mainly by fluorine motion, therefore, the NMR data obtained at higher temperatures can, in theory, provide information regarding the correlation time scale and activation energy of the relevant microscopic dynamical processes. As can be seen in Fig. 2, the observed narrowing of the NMR line emerges above 240 K and the line shape changes progressively from Gaussian (at $T=173$ K) towards Lorentzian (at $T=380$ K). In the intermediate region, the line shape is more complex and resembles a superposition of a narrow Lorentzian line and a broad Gaussian line (note the 298 K spectrum in Fig. 2). Such inhomogeneous narrowing process suggests the existence of fluorine species characterized by different mobility, being the narrow line associated to the fraction of mobile nuclei at that temperature. The criterion for motion narrowing is that the rate of fluctuation of the local fluorine dipolar fields, which is generally described in terms of a correlation time τ_s, become much greater than the rigid lattice linewidth expressed in frequency units, i.e., $\tau_s^{-1} \gg (\gamma^2 M_2)^{1/2}$.[28] Considering the $60PbGeO_3-20PbF_2-20CdF_2$ glass data we estimate $\tau_s \approx 1.7\times 10^{-5}$ s at the temperature corresponding to the onset of motional narrowing. As will be further discussed later, this value constitutes the lower value of the fluorine motional correlation time within the investigated temperature range. Finally, it should be noted that the onset of motional narrowing of the ^{19}F and ^{7}Li NMR line in fluorzirconate glasses is usually observed at higher temperatures; for example, at 300 K in $ZrF_4-BaF_2-LaF_3-AlF_3-LiF$ (ZBLALi) and at 400 K in $ZrF_4-BaF_2-LaF_3-AlF_3-NaF$ (ZBLAN).[32] Therefore, we may conclude that the fluorine ion mobility in our oxyfluoride glass is sufficiently high to average dipolar interactions at a lower temperature compared to fluorzirconate glasses.

3. Spin-lattice relaxation

Above room temperature, the ^{19}F spin-lattice relaxation rate is strongly influenced by the transport properties due to diffusive movements of F^- ions in the glass network. The relaxation process can be interpreted in terms of the fluctuations of the $^{19}F-^{19}F$ dipolar interaction resulting from the fluorine motion. The approach used in the Bloembergen–Purcell–Pound (BPP) model assumes noncorrelated isotropic random motions, yielding to a pair–pair spin correlation function of exponential form, $G_s(t)=\exp(-t/\tau_s)$, parameterized by the correlation time τ_s, which defines the time scale for changes of the local magnetic field experienced by the resonant nucleus.[28] In this context, the spectral density function, $J(\omega,\tau_s)$, given by the Fourier transform of the related correlation function, results

$$J(\omega,\tau_s)=\frac{\tau_s}{1+(\omega\tau_s)^2}. \tag{1}$$

The experimentally observable spin-lattice relaxation rate can be expressed in terms of the spectral density function evaluated at the NMR Larmor frequency, ω_0, and at its first harmonic, $2\omega_0$,[28,33]

$$T_1^{-1} \propto [J(\omega_0,\tau_s)+4J(2\omega_0,\tau_s)]. \tag{2}$$

In practice, the validity of the BPP model can be tested experimentally by verifying some of its main characteristic features: (i) T_1^{-1} should display a symmetric maximum at a temperature at which the condition $\omega_0\tau_s=0.62$ is fulfilled (usually approximated by $\omega_0\tau_s \approx 1$) and, (ii) at the low-temperature side of the maximum ($\omega_0\tau_s \gg 1$), the relaxation times should depend quadratically on the frequency ($T_1 \propto \omega_0^2\tau_s$).

For thermally activated processes such as ion diffusion in glasses, τ_s must be related to the individual ionic jump correlation time, τ_0, which is usually expressed by Arrhenius temperature dependence,

$$\tau_0=\tau_{0,\infty}e^{E_A/k_BT}. \tag{3}$$

Here, k_B is the Boltzmann constant, E_A is the microscopic barrier as seen by the hopping ion (or the activation energy for the process), and $1/\tau_{0,\infty}$ is the attempt frequency of the order of an optical phonon frequency ($10^{12}-10^{13}$ s^{-1}). For many physical systems, the condition $\tau_s=\tau_0$ can constitute a fair approximation, leading to an observable behavior with some additional features: (iii) when $\ln(T_1^{-1})$ is plotted against inverse temperature, the activation energy, E_A, can be determined from the slopes at either sides of the maximum, and (iv) if E_A is known, $\tau_{0,\infty}$ can be estimated from the maximum condition (i) and Eq. (3).

However, deviations from the BPP behavior are frequently encountered in disordered systems, where the T_1^{-1} dependence on frequency is weaker than ω_0^2 and asymmetric relaxation plots have been observed, with the slope on the high temperature side of the T_1^{-1} maximum being steeper than that on the low temperature side.[22,34,35] More probably, these observations indicate a nonexponential decay of the correlation function $G_s(t)$. A nonexponential decay may represent an ensemble average of exponential decays corresponding to a distribution of jump processes, each one with characteristic activation energy and correlation time.[22] Alternatively, it is also possible that the shape of the correlation function decay be inherently nonexponential, due to intrinsic cooperative interactions (mainly Coulomb interactions) among the mobile charged ions and their interaction with the glassy network.[23,36,37]

In the case of heavy metal fluoride glasses, the temperature dependence of the ^{19}F T_1^{-1} has been interpreted in terms of three main mechanisms: (a) spin relaxation processes attributed to low-frequency excitation of disorder modes, usually noticeable at temperatures below 300 K, (b) diffusive ionic motions which become significant in the region $300\text{ K} < T < T_g$, and (c) fast diffusive ionic motions, which are responsible for a ^{19}F spin-lattice relaxation rate maximum, generally localized at temperatures above T_g.[20,24,38,39]

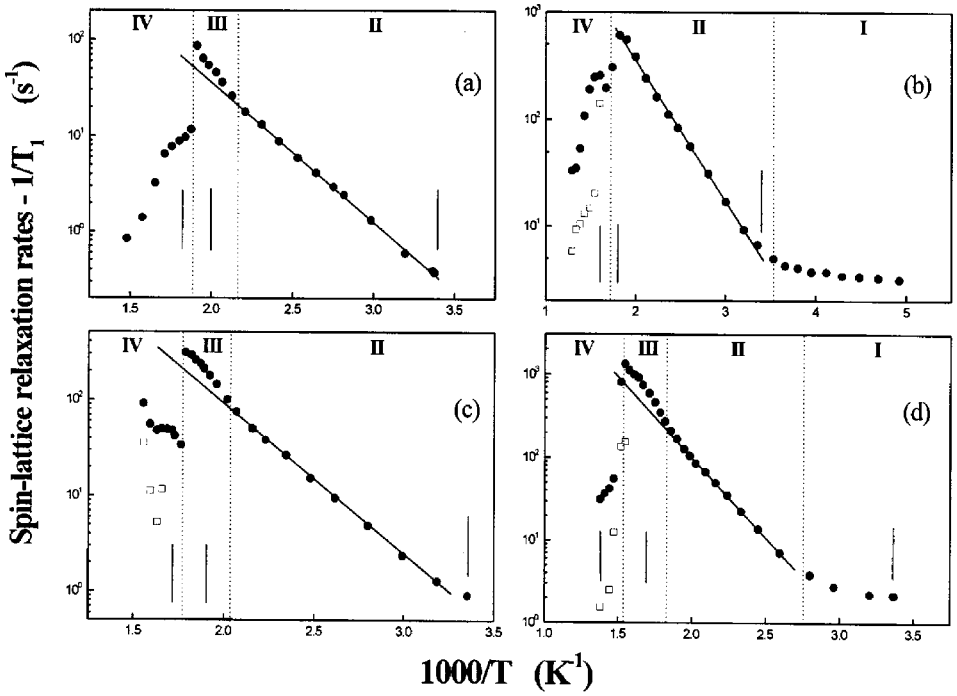

FIG. 3. Temperature dependence of the ^{19}F NMR spin-lattice relaxation rate ($1/T_1$) for the glasses: $60PbGeO_3-40PbF_2$ (a), $60PbGeO_3-20PbF_2-20CdF_2$ (b), $60PbGeO_3-30PbF_2-10CdF_2$ (c), and $60PbGeO_3-40CdF_2$ (d). All measurements were performed at the Larmor frequency of 36 MHz. The meaning of temperature regions I–IV are explained in the text. The short vertical lines indicate room temperature, T_g and T_x, respectively from right to left. For temperatures in region IV the relaxation recovery is fitted by a weighted sum of two exponential decays, associated to two time constants represented by symbols ● and □.

Before going any deeper in the theoretical foundations of the problem, we address to Fig. 3, where the temperature dependence of the ^{19}F spin-lattice relaxation rates (T_1^{-1}) of some of our studied glasses is plotted. In order to comment the main features of the relaxation curves shown in Fig. 3, it is useful to define temperature regions in which it is apparent that specific dynamic processes are ruling the spin relaxation. The limits of such temperature regions (as sketched with dashed lines in Fig. 3) are not exactly the same for all samples. By comparison, the characteristic temperatures determined by DSC, T_g and T_x, and the room temperature are also marked in Fig. 3. For all temperatures in the defined regions I, II, and III, the recoveries of the longitudinal magnetization towards equilibrium are described by exponential decays of time constant T_1.

In the temperature region I, below room temperature, the NMR relaxation rates exhibits weak temperature dependence, as seen clearly in Figs. 3(b) and 3(d). In region II the T_1^{-1} values increase with increasing temperature, closely following a straight line in the plots of Fig. 3. Increasing the temperature to inside region III, the data depart from the preceding straight-line behavior exhibiting a larger slope, with the inflection point at a temperature below T_g, denoted hereafter by T_m, which depends on the glass composition. Further increase of the temperature, toward the region IV, will cause an abrupt decrease of the T_1^{-1} values, resulting in an apparent discontinuity of the T_1^{-1} versus $1/T$ plot. The region III in Fig. 3(b) does not exists or seems to be too narrow to be identified. In region IV the magnetization recovery is, in all cases, nonexponential and well fitted by a weighted sum of two exponential functions with different time constants. Besides, due in part to a lower signal to noise ratio, the T_1 data obtained in this region is affected by a larger uncertainty.

A brief examination of the T_1^{-1} plots presented in Fig. 3 indicates that they cannot be completely understood within the framework of the BPP model. Starting from room temperature, T_1^{-1} increases with increasing temperature, however, a maximum in the T_1^{-1} temperature dependence is not observed. Indeed, it is apparent that before such maximum could be reached at some temperature above T_g, a sudden change in the T_1^{-1} behavior is observed, leading to nonexponential T_1 decays characterized by longer time constants. A more detailed discussion of the relaxation behavior on each region will be outlined in the following paragraphs.

In **region I**, individual fluorine ions mobility is too small to exert an influence on the nuclear relaxation process. A considerable number of NMR relaxation studies in inorganic glasses have found that T_1^{-1} increases monotonically with increasing temperature and depends sublinearly on the Larmor frequency. The process has been interpreted in the framework of thermally activated low-frequency excitations of disorder modes intrinsic to the glassy state of matter.[20,38–40] Since the microscopic structure of the disordered modes in glasses is unknown, they are commonly described on the basis of an asymmetric double-well potential configuration. Under these assumptions the spin-lattice relaxation rate has been expressed as a power law dependence on temperature and frequency, $T_1^{-1} \propto T^{\alpha}\omega^{-\gamma}$, with $1 \leqslant \alpha < 2$ and $0.5 \leqslant \gamma \leqslant 1.5$.

In **region II** of Fig. 3, diffusive fluorine motions play a

role in influencing nuclear relaxation processes. Although the exact nature of the relaxation mechanism is not well established at the moment, there is sufficient experimental evidence to support the idea that it corresponds to time-dependent fluctuations of the nuclear spin coupling between mutually interacting ion pairs, caused by thermally activated hopping motions of the charged particles in a disordered lattice.[23,36,37] The kind of approach used assumes that the Coulomb interaction among the ions and their interaction with the glassy network will cause the decay of the correlation function to slow down for times $t>1/\omega_c$, where ω_c denotes the characteristic frequency of the slowing-down process and is in the range $\omega_c \approx 10^{11}-10^{12}\ \mathrm{s}^{-1}$. In this scenario, the correlation function is well described by a stretched-exponential decay, denoted by $G_s(t) = \exp(-t/\tau_s)^{\beta}$. The stretching exponent, β, varies from 0 to 1. In a first approximation, the dependence of the resulting spectral density function with the frequency, ω, and correlation time, τ_s, is given by

$$J(\omega,\tau_s)=\frac{\tau_s}{1+(\omega\tau_s)^{1+\beta}}. \tag{4}$$

Switching off the Coulomb interaction, by taking low mobile ions concentrations, leads to $\beta=1$, recovering the BPP model. For any value of β, the relaxation rates in the slow ionic motion temperature region ($\omega_0\tau_s \gg 1$) can be approximated by a power law, $T_1 \propto \omega^{1+\beta}\tau_s^{\beta}$.

According to the coupling model,[37] the NMR correlation time, τ_s, is linked to the ionic jump correlation time, τ_0, given in Eq. (3), by

$$\tau_s=\tau_{s,\infty}e^{(E_A/\beta)/k_BT}=\left(\frac{\tau_{s,\infty}}{\tau_{0,\infty}}\right)\tau_0^{1/\beta}, \tag{5}$$

with,

$$\tau_{s,\infty}=[\beta\omega_c^{1-\beta}\tau_{0,\infty}]^{1/\beta}. \tag{6}$$

For $\beta=1$, we return to the simple behavior: $\tau_{s,\infty}=\tau_{0,\infty}$ and $\tau_s=\tau_0$.

When $\ln(T_1^{-1})$ is plotted against inverse temperature, Eqs. (2), (4), and (5) represent an asymmetric spin-lattice relaxation rate maximum, with asymptotic slopes given by $E_A/(\beta k_B T)$ at the high temperature side ($\omega_0\tau_s \ll 1$) and $-E_A/(k_BT)$ at the low temperature side ($\omega_0\tau_s \gg 1$). Recalling the experimental data of Fig. 3, and assuming that the condition $\omega_0\tau_s \gg 1$ is valid for the data of region II, activation energies (E_A) can be extracted from the slope of the relaxation plots and are in the range 0.28–0.38 eV, as listed in Table I.

According to Eqs. (4) and (5), the value of the asymmetry parameter, β, can only be estimated from the knowledge of the slopes in both sides of the relaxation maximum. However, as mentioned before, our experimental data shows no evidence that such maximum exists at temperatures below T_x. This means that, for temperatures below T_x, the correlation time is longer than the inverse of the Larmor frequency, $\tau_s > 0.62/\omega_0 = 2.7\times10^{-9}$ s. In general, it is recognized that ionic motions which are much too slow to be seen as a T_1^{-1} maximum (by using $\omega_0/2\pi$ in the MHz range) can be studied by measuring the spin-lattice relaxation rate in the rotating frame, denoted by $T_{1\rho}$. The theory predicts that a maximum in the $T_{1\rho}^{-1}$ versus T^{-1} plot should appear when the condition $2\omega_1\tau_s \approx 1$ is fulfilled, with $\omega_1/\gamma = H_1$ being the intensity of the radio-frequency magnetic field. We have implemented this idea by measuring $T_{1\rho}$ as a function of temperature for the glass $60PbGeO_3-20PbF_2-20CdF_2$ and the results are shown in Fig. 4.

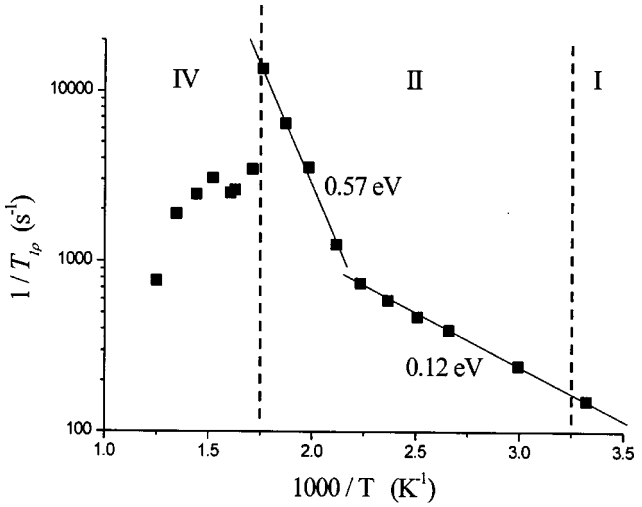

FIG. 4. Temperature dependence of the ^{19}F NMR spin-lattice relaxation rate in the rotating frame ($1/T_{1\rho}$) for the glass $60PbGeO_3-20PbF_2-20CdF_2$, measured at the frequency $\omega_1/2\pi \approx 20$ kHz. Temperature regions I, II, and IV are the same as determined from ($1/T_1$) measurements and are explained in the text.

As can be readily seen in Fig. 4, the maximum condition could not be reached. We have made no attempt to measure $T_{1\rho}$ for other glass compositions, but the experiment was performed twice with consistent results. However, the obtained data show some interesting features. First, and similar to the T_1 behavior, $T_{1\rho}^{-1}$ increases with increasing temperature in region II, but not following a single straight line. The average value of the activation energies obtained from the two linear slopes, as indicated in Fig. 4, is close to the value estimated from the single slope of the T_1^{-1} plot of Fig. 3. It is interesting to note that the change in the $T_{1\rho}^{-1}$ slope resembles the crossover between regions II and III, at temperature T_m, observed from ($1/T_1$) data in the other glass compositions. Second, characteristic features present in both T_1 and $T_{1\rho}$ data mark temperature region IV: nonexponential decays and irreproducible experimental data.

In Fig. 5 is shown the results obtained for the temperature dependence of the bulk conductivity of the glass $60PbGeO_3-20PbF_2-20CdF_2$. We note that the measured conductivity at, for example, 500 K is about 10^{-4} S/cm, which is one order of magnitude smaller than that measured in the superionic PbF_2.[33,41] However, this value is more than one order of magnitude higher than the conductivity measured in fluoride glasses at the same temperature.[36,42] It is interesting to note that in fluoride glasses the ^{19}F NMR relaxation rates increase very little between room temperature and T_g (e.g., from $\approx 2\ \mathrm{s}^{-1}$ at 300 K to $7\ \mathrm{s}^{-1}$ at T_g in fluorozirconate glass[24]). In contrast, the T_1^{-1} values, measured in our fluorogermanate glasses, increase almost three orders of magnitude between room temperature and T_g (Fig. 3), re-

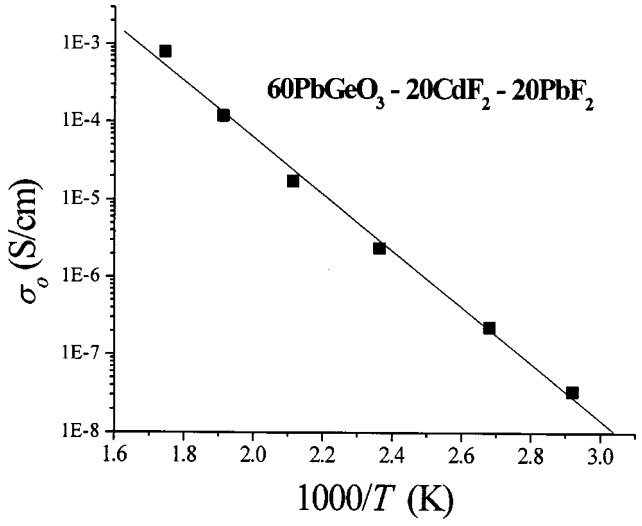

FIG. 5. Arrhenius plot of the bulk conductivity of the glass $60PbGeO_3-20PbF_2-20CdF_2$. The straight line is the least square fitting corresponding to an activation energy of ≈ 0.66 eV.

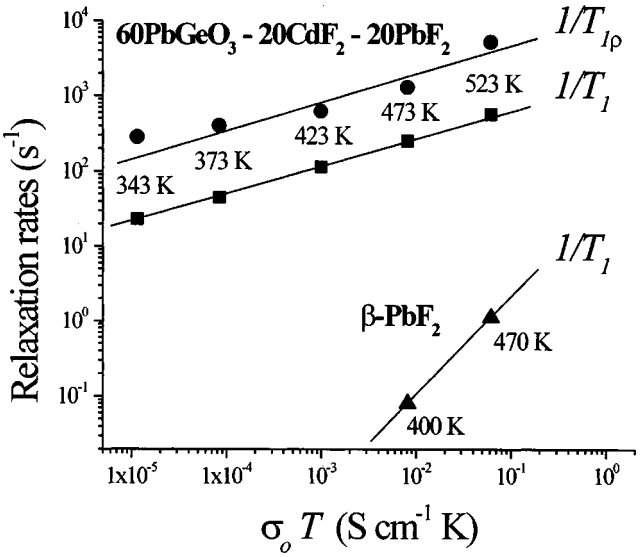

FIG. 6. Correlation between the spin-lattice relaxation rates ($1/T_{1\rho}$ at 20 kHz and $1/T_1$ at 36 MHz) and bulk conductivity times temperature ($\sigma_0 T$) of the glass $60PbGeO_3-20PbF_2-20CdF_2$. For comparison, the β-PbF_2 data extracted from Ref. 33 are schematically drawn. The straight lines are just guides to the eyes.

flecting the high ion mobility in these glasses at temperature region II.

Nuclear spin-lattice relaxation (NSLR) and electrical conductivity (EC) measurements probe the ionic motion in a different way, probably leading to different correlation functions for each property of the system. EC is equivalent to the ionic motion as a response to an external applied ac electrical field, whereas NSLR is the result of the longitudinal nuclear magnetization decay as a consequence of the ionic motion fluctuations. If these two properties of the system share a common correlation function, despite the physical differences in the correlations probed by NSLR and EC, the theorem of fluctuation-dissipation of statistical thermodynamics[43] suggests the following relation between NSLR and the real part of the complex ac conductivity, σ:

$$\frac{1}{T_1(\omega,T)}\alpha\frac{k_BT\sigma(\omega,T)}{\omega^2}. \tag{7}$$

This relation is to be applied only when the two properties are measured at the same temperature and frequency. Although, the relation (7) has been verified for various inorganic oxide glasses at low temperatures, the theoretical bases of a general correspondence between EC and NSLR experiments are still under discussion.[36,43]

The motion of ions in the glasses produces a non-Debye frequency dependence of the ac conductivity, which exhibits a power-law dependence at high frequencies but is constant at low frequencies, and can be described by[36,43,44]

$$\sigma T=\frac{1}{\tau_\sigma}[1+(\omega\tau_\sigma)^{1-\beta_\sigma}]. \tag{8}$$

Here, β_σ and τ_σ are, respectively, the correlation function exponent and the thermally activated correlation time associated with the conductivity process. From Eqs. (4) and (8), it can be readily seen that, in the slow ionic motion region ($\omega\tau_s, \omega\tau_\sigma \gg 1$), the approximation expressed in Eq. (7) leads to an equivalence of between the two exponents, β and β_σ, and also, to an linear relation between the correlation times τ_s and τ_σ.

However, notwithstanding the above-mentioned theoretical considerations, we call the attention that the frequency independent conductivity in Eq. (8), $\sigma_{dc}T\propto 1/\tau_\sigma$, is not affected by the exponent β_σ. Besides, assuming a linear relation between correlation times τ_s and τ_σ, $\sigma_{dc}T$ may be correlated with the NSLR rates measured at a constant frequency, $T_1^{-1}(\omega_0,T)\propto 1/(\tau_s)^\beta$. One example of such correlation is the case of the data obtained for the superionic cubic phase of β-PbF_2. For comparison, the PbF_2 data reproduced from literature[33] is plotted in Fig. 6, together with the data obtained for the glass of composition $60PbGeO_3-20PbF_2-20CdF_2$. One can notice that all the three sets of data follow approximate straight lines and, within experimental errors, the T_1 and $T_{1\rho}$ lines are parallel to each other in the case of our glass. Assuming an empirical relation of the form $T_1^{-1}\propto(\sigma_0 T)^\beta$ and comparing the three experimental straight lines, we found that the parameter $\beta \approx 1$ obtained for β-PbF_2 is greater than the value obtained for the glass sample, $\beta\approx 0.4\pm 0.1$.

The value of the slope obtained for the $60PbGeO_3-20PbF_2-20CdF_2$ glass in Fig. 6, $\beta\approx 0.4$, is of the same order than those reported for other inorganic glasses: CLAP glass ($CaF_2-LiF-AlF_3-PbF_2$, $\beta\approx 0.5$) and ZBLAN-20 glass ($27ZrF_4-27HfF_4-20BaF_2-3LaF_3-3AlF_3-20NaF$; $\beta\approx 0.3$).[36] The low-temperature activation energy $E_A=0.28$ eV obained for the $60PbGeO_3-20PbF_2-20CdF_2$ glass and the empirically found β value can be used to obtain the activation energy in the high temperature side, $E_\sigma^{dc}=E_A/\beta\approx 0.7$ eV. This value is close to that obtained from the conductivity data of Fig. 5 (0.66 eV).

The parameter $\tau_{0,\infty}$ defined in Eq. (3) can be calculated from the classical "oscillation frequency" f of a fluorine ion

in a potential modeled with a sinusoidal barrier shape of energy U_0 between wells separated by a distance d,[22,45]

$$f = d^{-1}\left(\frac{U_0}{2m}\right)^{1/2}, \tag{9}$$

where m is the mass of the ion under consideration and d is the average hopping distance, which is equivalent to the average F–F distance in the glass. Assuming a barrier energy equal to the fluorine motional activation energy ($U_0 = 0.66$ eV), Eq. (9) gives $f \approx 2\times10^{12}$ s^{-1}. This value—expressed in frequency units—is consistent with the ion motion bands measured by far-infrared spectroscopy in alkali germanate glasses (between 40–80 cm^{-1}, i.e., $1.2–2.4\times10^{12}$ s^{-1}) (Ref. 46) and is in good agreement with the optical phonon frequency measured in β-PbF_2 ($\approx$100 cm^{-1} or 3×10^{12} s^{-1}) and CdF_2 ($\approx$215 cm^{-1} or 6.5×10^{12} s^{-1}).[47] Assuming a cutoff frequency ω_c of the order of 10^{12} s^{-1} and $\tau_{0,\infty} = 1/f \approx 5\times10^{-13}$ s, Eq. (6) gives a prefactor $\tau_{s,\infty} \approx 1.8\times10^{-14}$ s. Finally, the order of magnitude of the fluorine motional correlation time at the onset of the glass transition temperature, can be calculated from Eq. (5), yielding $\tau_s \approx 10^{-7}$ s at 530 K.

The estimated correlation time ($\tau_s \approx 10^{-7}$ s at 530 K) is the result of simplifying assumptions but its order of magnitude is consistent with the high ionic mobility observed in the fluorogermanate glasses studied here, and with the large ^{19}F T_1^{-1} increase between $\approx$340 K and T_g. It should be noted that in the fast ionic conductor PbF_2, the correlation time obtained from multifrequency ^{19}F NMR relaxation experiments is $\tau \approx 10^{-7}$ s at the same temperature ($\approx$480 K) where the measured conductivity reaches $\approx 2\times10^{-4}$ S/cm.[33] In summary, these results and the fact that the relaxation process is exponential below T_g suggests that transport and relaxation in these particular glasses involve microscopic processes possesing characteristic time scale similar to those found in fluoride crystals.

The activation energy values, deduced from the slope of the relaxation plot of **region III**, are between 0.6 and 0.75 eV, showing a substantial increase with respect to the values obtained from region II (Table I). This could be easily understood if the increase in temperature, when going from region II to region III, induced faster fluorine motions that could strongly influence the relaxation process. However, it must be noted that a similar increase in the fluorine mobility has been observed in most fluoride and inorganic glasses only above the glass transition temperature.[24,40] In contrast, the supposed influence of fast ionic motions in the relaxation data of region III become evident at temperatures 40 to 50 K below T_g, what could be understood only if the fluorine mobility in our oxyfluoride glasses is higher than that observed for fluoride glasses. To get support for our discussion, we recall the case of the fast ionic conductor PbF_2, where the conductivity in the range 300–550 K is due to intrinsic defects named anion Frenkel pairs, or, anion vacancies and anions in the cubic centered interstitial sites. The activation energy determined from the conductivity data in this temperature region is $\approx$0.74 eV. In the region 550–750 K a substantial change in the slope of the conductivity curve of PbF_2 is observed, which is attributed to motion of interstitial fluoride ions, with activation energy of $\approx$1 eV.[33,41] To compare such observations with our data, we call attention that the low temperature limit of region III in Fig. 4, T_m, depends on the relative content of PbF_2 and CdF_2 in the glass composition and shifts toward lower temperatures as the PbF_2 content increases. In fact, CdF_2 is a poor ionic conductor compared to PbF_2.[48,49] Provided that the activation energies obtained from the nuclear relaxation are quite similar (between 0.28 and 0.38 eV) one can compare the relative mobility of the fluorine ions of our different glasses by comparing their respective T_m. Therefore, it seems reasonable to conclude that the fluorine mobility in the glass $60PbGeO_3–40PbF_2$ ($T_m \approx 460$ K) is higher than that in the $60PbGeO_3–40CdF_2$ glass ($T_m \approx 530$ K).

The temperature **region IV** is characterized by an abrupt change of the NMR relaxation behavior. As the temperature is increased to around the onset of crystallization, T_x, a discontinuity on the relaxation curves (T_1 and $T_{1\rho}$) is observed for all studied samples. The acquired data in this region is less reproducible than the rest, in the sense that, if a new run is performed with a fresh sample the temperature at which the discontinuity appears remains the same, but the acquired relaxation values may present relative differences of almost one order of magnitude. As mentioned before, the relaxation recovery in region IV is evidently nonexponential and the signal to noise ratio is smaller than that for the rest of the data. Such behavior must be related to the crystallization processes, which begins to develop above T_x. The crystallization process leads to the segregation of phases and interfaces between the created crystalline phases and the remaining amorphous material. Therefore, we conclude that the fluorine motion must be conditioned to this new material structure and may follow a different dynamics, characterized by new values of correlation times and activation energies. To our knowledge, there are no previous reports of such NMR observation in glassy systems. We have found in the literature only one example where a similar discontinuity is observed in EC data above T_g, which was attributed to deformations due to a softening of the sample.[50]

To better understand the effect of crystallization on the ionic transport properties, we undertake a systematic NMR investigation of our samples after thermal treatment, giving rise to glass-ceramics material. The results show that the temperature dependence of T_1 reflects the existence of at least two fluorine species with different mobility. In fact, the crystallization process plays a dominant role in affecting the ionic mobility. This matter will is the subject of our subsequent reports.

IV. CONCLUSION

Raman and EXAFS data suggest the existence of a heterogeneous structure at the molecular scale for glasses in the system $PbGeO_3–PbF_2–CdF_2$. A metagermanate chain, similar to the one found in the monoclinic $PbGeO_3$, is suggested to be the basic structural feature for the lead–cadmium fluorogermanate glasses studied here. The addition of metal fluorides leads to the substitution of nonbridging fluoride atoms for bridging oxygen atoms. ^{19}F NMR data analysis lead to

F–F distances similar to the ones found in pure crystalline phases, suggesting that fluorine rich regions are permeating the metagermanate chains, in accordance with the Raman and EXAFS analysis. Due to an incomplete knowledge of the microscopic structure, the conduction mechanism in the fluorogermanate glasses studied here is still not fully understood, nevertheless, we can state that the ionic transport takes place along microscopic pathways in the fluorine rich region of the glass and, furthermore, the existence of a connectivity network of pathways on a microscopic scale seems to be assured by the high fluorine concentration in the glass composition. This assumption may give support to the electric conductivity and NMR data analysis, which indicate that the cadmium–lead flurogermanate glasses studied here are fairly good ionic conductors. Also, we may speculate that such fluorine rich regions can present favorable thermodynamic environment for the nucleation of nanocrystalline domains, typical of those found in the ultra transparent glass-ceramics that can be prepared from these oxifluoride glasses The difficulties found for the analysis of the NMR relaxation data, and its correspondence with the electrical conductivity data, is inherent to the properties of this glassy system, indicating, once more, that the available theoretical basis and experimental techniques are not sufficient to obtain a complete picture of the relationship between ionic mobility and the structure of the glass.

ACKNOWLEDGMENTS

This research was partially supported by LNLS-National Synchrotron Light Laboratory, Brazil. The financial support of Brazilian agencies Fapesp, Capes and CNPq is also gratefully acknowledged. The ''LEM'' laboratory (Institute of Chemistry-USP-São Paulo, Brazil) is acknowledged for the permission in using their Raman facilities.

[1] Y. Wang, A. Osaka, and Y. Miura, J. Non-Cryst. Solids **112**, 323 (1989).
[2] J. Coon, M. Horton, and J.E. Shelby, J. Non-Cryst. Solids **102**, 143 (1988).
[3] S. Goldammer, A. Runge, and H. Kahnt, Solid State Ionics **70/71**, 380 (1994).
[4] R. Gopalakrishnan, B.V.R. Chowdari, and K.L. Tan, Solid State Ionics **51**, 203 (1992).
[5] G. El-Damrawi, Phys. Status Solidi A **177**, 385 (2000).
[6] R. Higginbottom and J.E. Shelby, Phys. Chem. Glasses **39(5)**, 281 (1998).
[7] Y. Wang and J. Ohwaki, Appl. Phys. Lett. **63**, 24 (1993).
[8] P.A. Tick, N.F. Borreli, L.K. Cornelius, and M.A. Newhouse, J. Appl. Phys. **78**, 6367 (1995).
[9] P.A. Tick, N.F. Borrelli, and I.M. Reaney, Opt. Mater. (Amsterdam, Neth.) **15**, 81 (2000).
[10] J. Qiu, R. Kanno, Y. Kawamoto, Y. Bando, and K. Kurashima, J. Mater. Sci. Lett. **17(8)**, 653 (1998).
[11] L.A. Bueno, P. Melnikov, Y. Messaddeq, and S.J.L. Ribeiro, J. Non-Cryst. Solids **247**, 87 (1999).
[12] M. Mortier and F. Auzel, J. Non-Cryst. Solids **256/257**, 361 (1999).
[13] J. Mendes-Ramos, V. Lavin, I.R. Martin, U.R. Rodriguez-Mendoza, J.A. Gonzales-Almeida, V.D. Rodriguez, A.D. Lozano-Gorrin, and P. Nunez, J. Alloys Compd. **323/324**, 753 (2001).
[14] M.A.P. Silva, Y. Messaddeq, V. Briois, M. Poulain, and S.J.L. Ribeiro, J. Braz. Chem. Soc., **13(2)**, 200 (2002).
[15] M.A.P. Silva, V. Briois, M. Poulain, Y. Messaddeq, and S.J.L. Ribeiro, J. Phys. Chem. Solids **64(1)**, 95 (2003).
[16] B. Bureau, G. Silly, J.Y. Buzaré, J. Emery, C. Legein, and C. Jacoboni, J. Phys.: Condens. Matter **9**, 6719 (1997).
[17] J.M. Bobe, J. Senegas, J.M. Reau, and M. Polain, J. Non-Cryst. Solids **162**, 169 (1993).
[18] D. Brinkmann, Prog. Nucl. Magn. Reson. Spectrosc. **24**, 527 (1992).
[19] D. Lathrop and H. Eckert, J. Am. Chem. Soc. **111**, 3536 (1989).
[20] O. Kanert, J. Dieckhöfer, and R. Küchler, J. Non-Cryst. Solids **203**, 252 (1996).
[21] P. Mustarelli, C. Tomasi, A. Magistris, and M. Cutroni, J. Non-Cryst. Solids **232–234**, 532 (1998).
[22] S. Sen and J.F. Stebins, Phys. Rev. B **55**, 3512 (1997).
[23] S. Sen and T. Mukerji, J. Non-Cryst. Solids **293–295**, 268 (2001).
[24] T. Auler, J.P. Donoso, P.L. Frare, C.J. Magon, Y. Messaddeq, and A.A.S.T. Delben, J. Non-Cryst. Solids **247**, 92 (1999).
[25] O. Yamaguchi, K. Sugiura, M. Muto, and K. Shimizu, Z. Anorg. Allg. Chem. **525**, 230 (1985).
[26] S.J.L. Ribeiro, J. Dexpert-Ghys, B. Piriou, and V. Mastelaro, J. Non-Cryst. Solids **159**, 213 (1993).
[27] B. Lengeler and P. Eisenberger, Phys. Rev. B **21**, 4507 (1980).
[28] A. Abragam, *Principles of Nuclear Magnetism* (Oxford University Press, London, 1961).
[29] J.W. Zwanziger, J.C. McLaughlin, and S.L. Tagg, Phys. Rev. B **56**, 5243 (1997).
[30] J. Schooman, L.B. Ebert, C-H. Hsieh, and R. Huggins, J. Appl. Phys. **46**(7), 2873 (1975).
[31] I. Kosacki and E. Dynowska, J. Cryst. Growth **50**, 575 (1980).
[32] S. Estalji, R. Küchler, O. Kanert, R. Bölter, H. Jain, and K.L. Ngai, J. Phys. IV **2(C2)**, 159 (1992).
[33] J.B. Boyce and B.A. Huberman, Phys. Rep. **51**(4), 189 (1979).
[34] M. Tatsumisago and C.A. Angell, J. Chem. Phys. **97**, 6968 (1992).
[35] M. Meyer, P. Maass, and A. Bunde, Phys. Rev. Lett. **71**, 573 (1993).
[36] O. Kanert, R. Küchler, K.L. Ngai, and H. Jain, Phys. Rev. B **49**, 76 (1994).
[37] K.L. Ngai, J. Phys. Chem. A **98**, 6424 (1993).
[38] J. Dieckhöfer, O. Kanert, R. Küchler, and A. Volmari, Phys. Rev. B **55**, 14836 (1997).
[39] X. Lu, H. Jain, O. Kanert, R. Küchler, and J. Dieckhöfer, Philos. Mag. B **70(5)**, 1045 (1994).
[40] R. Küchler, O. Kanert, M. Fricke, H. Jain, and K.L. Ngai, J. Non-Cryst. Solids **172–174**, 1373 (1994).
[41] G.A. Samara, J. Phys. Chem. Solids **40**, 504 (1979).
[42] W.C. Hasz, C.T. Moyniham, and P.A. Tick, J. Non-Cryst. Solids **172–174**, 1363 (1994).
[43] D.L. Sidebottom, P.F. Green, and R.K. Brow, J. Chem. Phys. **108**, 5870 (1998).
[44] M. Cutroni, A. Mandanici, P. Mustarelli, C. Tomasi, and M. Federico, J. Non-Cryst. Solids **307–310**, 963 (2002).
[45] Bohnke, J. Emery, A. Veron, J.L. Fourquet, J.Y. Buzaré, P. Florian, and D. Massiot, Solid State Ionics **109**, 25 (1998).
[46] E.I. Kamitsos, Y.D. Yiannopoulos, H. Jain, and W.C. Huang, Phys. Rev. B **54**, 9775 (1996).
[47] I. Kosacki, Appl. Phys. A: Solids Surf. **49**, 413 (1989).
[48] A. Kessler and J.E. Caffyn, J. Phys. C **5**, 1134 (1972).
[49] P. Suptitz, E. Brink, and D. Becker, Phys. Status Solidi B **54**, 713 (1972).
[50] M. Teke and A. Chadwick, Mater. Sci. Forum **239–241**, 421 (1997).